

# A revised hydrology for the ECMWF model: Verification from field site to terrestrial water storage and impact in the Integrated Forecast System

G. Balsamo<sup>1</sup>, P. Viterbo<sup>2</sup>, A. Beljaars<sup>1</sup>,  
B. van den Hurk<sup>3</sup>, M. Hirschi<sup>4</sup>,  
A. K. Betts<sup>5</sup>, K. Scipal<sup>1</sup>

Research Department

<sup>1</sup>ECMWF, UK, <sup>2</sup>IM, Lisbon, Portugal,  
<sup>3</sup> KNMI, DeBilt, The Netherlands, <sup>4</sup>ETH-Zurich, Switzerland,  
<sup>5</sup>Atmospheric Research, Pittsford, Vermont, USA

submitted to *Journal of Hydrometeorology*

April 2008

*This paper has not been published and should be regarded as an Internal Report from ECMWF.  
Permission to quote from it should be obtained from the ECMWF.*



European Centre for Medium-Range Weather Forecasts  
Europäisches Zentrum für mittelfristige Wettervorhersage  
Centre européen pour les prévisions météorologiques à moyen terme

Series: ECMWF Technical Memoranda

A full list of ECMWF Publications can be found on our web site under:

<http://www.ecmwf.int/publications/>

Contact: [library@ecmwf.int](mailto:library@ecmwf.int)

©Copyright 2008

European Centre for Medium-Range Weather Forecasts  
Shinfield Park, Reading, RG2 9AX, England

Literary and scientific copyrights belong to ECMWF and are reserved in all countries. This publication is not to be reprinted or translated in whole or in part without the written permission of the Director. Appropriate non-commercial use will normally be granted under the condition that reference is made to ECMWF.

The information within this publication is given in good faith and considered to be true, but ECMWF accepts no liability for error, omission and for loss or damage arising from its use.

## Abstract

The Tiled ECMWF Scheme for Surface Exchanges over Land (TESSEL) is used operationally in the Integrated Forecast System (IFS) for describing the evolution of soil, vegetation and snow over the continents at diverse spatial resolutions. A revised land surface hydrology (HTESSEL) is introduced in the ECMWF operational model, to address shortcomings of the land surface scheme, specifically the lack of surface runoff and the choice of a global uniform soil texture. New infiltration and runoff schemes are introduced with a dependency on the soil texture and standard deviation of orography. A set of experiments in stand-alone mode is used to assess the improved prediction of soil moisture at local scale against field site observations. Comparison with Basin-Scale Water Budget (BSWB) and Global Runoff Data Centre (GRDC) datasets indicates a consistently larger dynamical range of land water mass over large continental areas, and an improved prediction of river runoff, while the impact on atmospheric fluxes is fairly small. Finally the ECMWF data assimilation and prediction systems are used to verify the impact on surface and near-surface quantities in atmospheric-coupled mode. A mid-latitude error reduction is seen both in soil moisture and in 2m temperature.

## 1. Introduction

A correct representation of the soil water buffering in land surface schemes used for weather and climate prediction is essential to accurately simulate surface water fluxes both towards the atmosphere and rivers ([van den Hurk et al., 2005](#); [Hirschi et al., 2006a](#)). Moreover the energy repartition at the surface is largely driven by the soil moisture which influences directly the Bowen ratio.

The introduction of a revised hydrology in the Tiled ECMWF Scheme for Surface Exchanges over Land (TESSEL) has been investigated by [van den Hurk and Viterbo \(2003\)](#) for the Baltic basin. These model developments were a response to known weaknesses of the TESSEL hydrology: specifically the choice of a single global soil texture, which does not characterize different soil moisture regimes, and a Hortonian runoff scheme which produces hardly any surface runoff. A revised formulation of the soil hydrological conductivity and diffusivity, spatially variable according to a global soil texture map, and surface runoff based on the variable infiltration capacity approach, are the proposed remedies.

Offline (or stand-alone) verification is a convenient framework for isolating the benefits of a given land surface parameterization. A set of field site experiments and two land surface intercomparison experiments over large domains are considered. A Sahelian site and a Boreal forest site have been chosen to show relevant effects of the new hydrology. Two major land surface intercomparison experiments, the Global Soil Wetness Project, Second initiative, GSWP-2 ([Dirmeier et al., 1999, 2002](#); [Gao et al., 2004](#)) and the Rhône Aggregation Project, RhôneAgg ([Boone et al., 2004](#)), provided spatialized near-surface forcing for land surface models, and have been re-run with the new scheme to evaluate the water budget for accumulated quantities. In the GSWP-2 simulations, both terrestrial water storage estimates and the river discharge are examined on a number of basins. Hydrological consistency on the monthly time-scale is verified. The RhôneAgg simulation are used to examine the fast component of runoff at the daily time-scale.

The coupling between the land surface and the atmosphere is then also evaluated. This is an essential step, since [Koster et al. \(2004\)](#) indicated a strong inter-model variability in coupling between soil moisture and precipitation over large continental areas, generalizing the studies of [Beljaars et al. \(1996\)](#).

In order to assess the impact of the new parameterization, a set of long-term atmospheric coupled integrations (13-month) with specified Sea-Surface-Temperature is produced. This configuration, named *climate simulation* allows evaluating surface-atmosphere feedbacks and focusing on the impact of the land surface modification. Annual and seasonal averages are compared to a number of independent datasets with a focus on boreal summer months when a larger impact of the soil hydrology is expected. Finally, since in the NWP application the

coupled system is subject to cyclic correction by data assimilation, an overall assessment is provided by the comparison of the land surface analysis increments in the old and new version of the land surface model. A reduction of increments between the two model versions can be interpreted as an overall improvement of the land surface representation. In this case the soil moisture increments are considered in a long (7-month) data assimilation experiment.

In section 2 the hydrology of the TESSEL land surface scheme and the HTESSEL (Hydrology TESSEL) revision are illustrated. Sensitivity experiments are realized to show the impact of the new parameterization on surface runoff and soil water transfer. Section 3 evaluates the soil moisture range associated with the new physiographic values (for the permanent wilting point and the soil field capacity) for a number of sites and presents the validation results at two contrasting field sites that illustrate the main behaviour of the HTESSEL and TESSEL scheme. In section 4, the regional to global offline simulations are introduced, together with the main verification datasets provided by the Basin-Scale Water Budget, BSWB (Seneviratne et al., 2004) the Global Runoff Data Centre, GRDC (Fekete et al., 2000) and the ERA-40 reanalysis (Uppala et al., 2005) datasets.

Results of atmospheric-coupled simulations and data assimilation experiments are presented and discussed in section 5 together with the relevant lessons learnt from the ERA-40 reanalysis. A summary of the changes and the conclusions are then provided in the last section, while the datasets for the global implementation of the revised hydrology scheme are presented in the Appendix.

## 2. TESSEL hydrology

The TESSEL scheme (Tiled ECMWF Scheme for Surface Exchanges over Land) is shown schematically in Figure 1a. Up to six tiles are present over land (bare ground, low and high vegetation, intercepted water, shaded and exposed snow) and 2 over water (open and frozen water) with separate energy and water balances. The

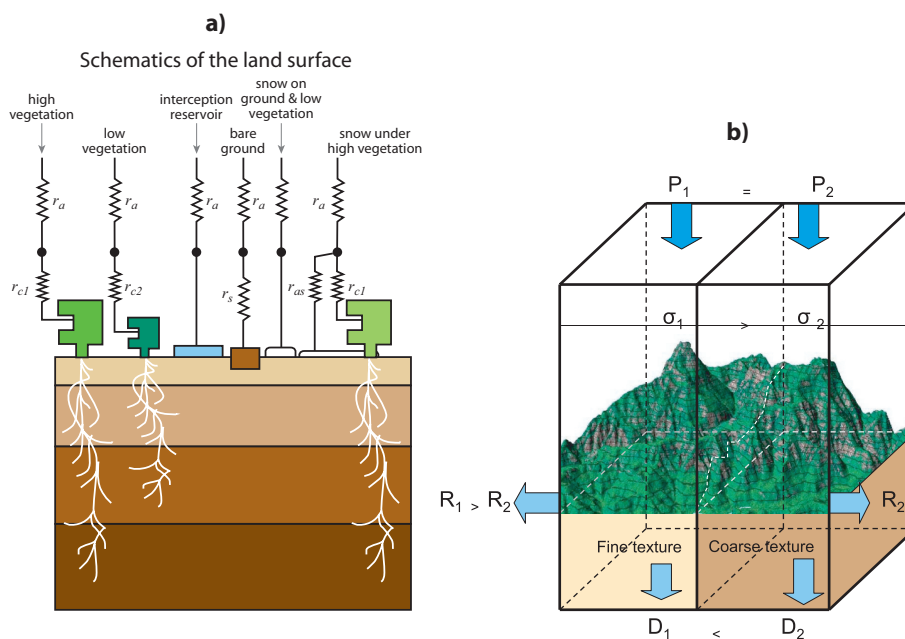


Figure 1: Schematic representation of the structure of (a) TESSEL land-surface scheme and (b) spatial structure added in HTESSEL (for a given precipitation  $P_1 = P_2$  the scheme distributes the water as surface runoff and drainage with functional dependencies on orography and soil texture respectively).

vertical discretization considers a four-layer soil that can be covered by a single layer of snow. The depths of the soil layers are in an approximate geometric relation, as suggested in [Deardorff \(1978\)](#). [Warrilow et al. \(1986\)](#) have shown that four layers provide a reasonable compromise between computational cost and the ability to represent all timescales between one day and a year. The soil heat budget follows a Fourier diffusion law, modified to take into account soil water freezing/melting according to [Viterbo et al. \(1999\)](#). The energy equation is solved with a net ground heat flux as the top boundary condition and a zero-flux at the bottom. An interception layer accumulates precipitation until it is saturated, and the remaining precipitation (throughfall) is partitioned between surface runoff and infiltration. Subsurface water fluxes are determined by Darcy's law, used in a soil water equation solved with a four-layer discretization shared with the heat budget equation. The top boundary condition is infiltration plus surface evaporation, free drainage is assumed at the bottom and each layer has an additional sink of water in the form of root extraction over vegetated areas.

In each grid box two vegetation types are present: a high and a low vegetation type. An external climate database is used to obtain the vegetation characteristics, based on the Global Land Cover Characteristics (GLCC) data ([Loveland et al., 2000](#)), <http://edcsns17.cr.usgs.gov/glcc/>. The nominal resolution is 1 km. The data provides for each pixel a biome classification based on the Biosphere-Atmosphere Transfer Scheme (BATS) model ([Dickinson et al., 1993](#)), and four parameters have been derived for each grid box: dominant vegetation type,  $T_H$  and  $T_L$ , and the area fraction,  $A_H$  and  $A_L$ , for each of the high- and low-vegetation components, respectively.

The vertical movement of water in the unsaturated zone of the soil matrix obeys the following equation ([Richards, 1931](#); [Philip, 1957](#); [Hillel, 1982](#); [Milly, 1982](#)) for the volumetric water content  $\theta$ :

$$\rho_w \frac{\partial \theta}{\partial t} = -\frac{\partial F_w}{\partial z} + \rho_w S_\theta \quad (1)$$

where  $\rho_w$  is the water density ( $\text{kg m}^{-3}$ ),  $F_w$  is the water flux in the soil (positive downwards,  $\text{kg m}^{-2}\text{s}^{-1}$ ), and  $S_\theta$  is a volumetric sink term associated to root uptake ( $\text{m}^3\text{m}^{-3}\text{s}^{-1}$ ), which depends on the surface energy balance and the root profile ([Viterbo and Beljaars, 1995](#)).

The liquid water flow,  $F_w$ , obeys Darcy's law, written as

$$F_w = -\rho_w \left( \lambda \frac{\partial \theta}{\partial z} - \gamma \right) \quad (2)$$

where  $\lambda$  ( $\text{m}^2 \text{s}^{-1}$ ) and  $\gamma$  ( $\text{m s}^{-1}$ ) are the hydraulic diffusivity and hydraulic conductivity, respectively.

Replacing (2) in (1), and defining parametric relations for  $\lambda$  and  $\gamma$  as functions of soil water, a partial differential equation for  $\theta$  is obtained:

$$\frac{\partial \theta}{\partial t} = \frac{\partial}{\partial z} \left( \lambda \frac{\partial \theta}{\partial z} - \gamma \right) + S_\theta \quad (3)$$

The top boundary condition is given by precipitation plus snow melt minus bare ground evaporation minus surface runoff. The bottom boundary condition assumes free drainage. [Abramopoulos et al. \(1988\)](#) specified free drainage or no drainage, depending on a comparison of a specified geographical distribution of bedrock depth, with a model-derived water-table depth. For the sake of simplicity the assumption of no bedrock everywhere has been adopted.

TESSEL adopts the [Clapp and Hornberger \(1978\)](#) formulation of hydraulic conductivity and diffusivity as a function of soil-water content (see also [Mahrt and Pan 1984](#) for a comparison of several formulations and

Cosby et al. 1984 for further analysis)

$$\begin{aligned}\gamma &= \gamma_{\text{sat}} \left( \frac{\theta}{\theta_{\text{sat}}} \right)^{2b_c+3} \\ \lambda &= \frac{b_c \gamma_{\text{sat}} (-\psi_{\text{sat}})}{\theta_{\text{sat}}} \left( \frac{\theta}{\theta_{\text{sat}}} \right)^{b_c+2}\end{aligned}\quad (4)$$

where  $b_c$  is a non-dimensional exponent,  $\gamma_{\text{sat}}$  and  $\psi_{\text{sat}}$  are the values of the hydraulic conductivity and matric potential at saturation. A minimum value is assumed for  $\lambda$  and  $\gamma$  corresponding to permanent wilting-point water content.

Cosby et al. (1984) tabulate best estimates of  $b_c$ ,  $\gamma_{\text{sat}}$ ,  $\psi_{\text{sat}}$  and  $\theta_{\text{sat}}$ , for the 11 soil classes of the US Department of Agriculture (USDA) soil classification, based on measurements over large samples. Viterbo and Beljaars (1995) adopted an averaging procedure to calculate for a medium-textured (loamy) soil used in TESSEL the values of  $\gamma_{\text{sat}} = 0.57 \times 10^{-6} \text{ m s}^{-1}$ ,  $b_c = 6.04$ , and  $\psi_{\text{sat}} = -0.338 \text{ m}$ , compatible with the Clapp and Hornberger expression for the matric potential

$$\psi = \psi_{\text{sat}} \left( \frac{\theta}{\theta_{\text{sat}}} \right)^{-b_c} \quad (5)$$

with  $\psi(\theta_{\text{pwp}}) = -153 \text{ m}$  ( $-15 \text{ bar}$ ) and  $\psi(\theta_{\text{cap}}) = -3.37 \text{ m}$  ( $-0.33 \text{ bar}$ ) (following Hillel 1982 and Jacquemin and Noilhan 1990).

The water transport in frozen soil is limited in the case of a partially frozen soil, by considering the effective hydraulic conductivity and diffusivity to be a weighted average of the values for total soil water and a very small value (for convenience, taken as the value of (Eq. 4) at the permanent wilting point) for frozen water as detailed in Viterbo et al. (1999). The soil properties, as defined above, also imply a maximum infiltration rate at the surface defined by the maximum downward diffusion from a saturated surface. In general when the water flux at the surface exceeds the maximum infiltration rate, the excess water is put into surface runoff. The general formulation of surface runoff can be written as:

$$R = T + M - I_{\text{max}} \quad (6)$$

where  $I_{\text{max}}$  is the maximum infiltration rate,  $T$  the throughfall precipitation and  $M$  the snow melting. Different runoff schemes differ in the formulation of the infiltration. The maximum infiltration or Hortonian runoff, represent the runoff process at local scales. In TESSEL the maximum infiltration rate  $I_{\text{max}}$  is calculated as

$$I_{\text{max}} = \rho_w \left( \frac{b_c \gamma_{\text{sat}} (-\psi_{\text{sat}})}{\theta_{\text{sat}}} \frac{\theta_{\text{sat}} - \theta_1}{z_1/2} + \gamma_{\text{sat}} \right) \quad (7)$$

where  $\rho_w$  is the water density, and  $z_1$  is the depth of the first soil model layer (7 cm). At typical NWP model resolutions this scheme is active only in the presence of frozen soil, when downward soil water transfer is inhibited, otherwise it hardly ever produces runoff, as shown in Boone et al. (2004).

#### a. The HTESSEL revision

The HTESSEL scheme includes the following revisions to the soil hydrology: (i) a spatially varying soil type replacing the single loamy soil, (ii) the Van Genuchten (VG) formulation of soil hydraulic properties replacing the Clapp and Hornberger (CH) scheme, and (iii) the surface runoff generation changing according to a variable infiltration capacity based on soil type and local topography.

Table 1: Van Genuchten soil parameters.

Texture	$\alpha$	$l$	$n$	$\gamma_{sat}$
Units	$m^{-1}$	-	-	$10^{-6}m/s$
Coarse	3.83	1.250	1.38	6.94
Medium	3.14	-2.342	1.28	1.16
Medium-Fine	0.83	-0.588	1.25	0.26
Fine	3.67	-1.977	1.10	2.87
Very Fine	2.65	2.500	1.10	1.74
Organic	1.30	0.400	1.20	0.93

Table 2: Values for the volumetric soil moisture in Van Genuchten and Clapp-Hornberger (CH, loamy; bottom row), at saturation,  $\theta_{sat}$ , field capacity,  $\theta_{cap}$ , and permanent wilting point,  $\theta_{pwp}$ . Last column reports the plant available soil moisture. Units are  $[m^3m^{-3}]$ .

Texture	$\theta_{sat}$	$\theta_{cap}$	$\theta_{pwp}$	$\theta_{cap} - \theta_{pwp}$
Coarse	0.403	0.244	0.059	0.185
Medium	0.439	0.347	0.151	0.196
Medium-Fine	0.430	0.383	0.133	0.251
Fine	0.520	0.448	0.279	0.170
Very Fine	0.614	0.541	0.335	0.207
Organic	0.766	0.663	0.267	0.396
Loamy (CH)	0.472	0.323	0.171	0.151

In Figure 1b the HTESSSEL changes are illustrated: in two adjacent model grid-points with the same land surface conditions and receiving an equal amount of precipitation the surface runoff will be different and proportional to the terrain complexity while the soil water drainage will depend on the soil texture class.

The van Genuchten (1980) formulation provides a closed-form analytical expression for the conductivity, given as a function of the pressure head,  $h$ , as

$$\gamma = \gamma_{sat} \frac{[(1 + \alpha h^n)^{1-1/n} - \alpha h^{n-1}]^2}{(1 + \alpha h^n)^{(1-1/n)(l+2)}} \quad (8)$$

where  $\alpha$ ,  $n$  and  $l$  are soil-texture dependent parameters. Pressure head  $h$  is linked to the soil moisture by the expression

$$\theta(h) = \theta_r + \frac{\theta_{sat} - \theta_r}{(1 + \alpha h)^{1-1/n}} \quad (9)$$

The VG scheme is recognized among soil physicists as capable of reproducing both the soil water retention and the hydraulic conductivity, and has shown good agreement with observations in intercomparison studies (Shao and Irannejad, 1999). Table 1 lists parameter values for six soil textures for the VG scheme. HTESSSEL uses the dominant soil texture class for each gridpoint. This information is taken from the FAO (FAO, 2003) dataset as detailed in the Appendix. The permanent wilting point and the soil field capacity are obtained by a specified matric potential of  $\psi(\theta_{pwp}) = -15\text{bar}$  and  $\psi(\theta_{cap}) = -0.10\text{bar}$ , respectively. In Table 2 the volumetric soil moistures associated with each soil class are shown for saturation, field capacity and wilting point. Also shown is the plant available water content and the percentage of land points in each class. The last row shows the corresponding values for the single loamy soil used in the CH formulation in TESSEL. Note that the plant available soil water is greater for all the new soil classes in HTESSSEL. Figure 2 shows the soil hydraulic diffusivity and conductivity for the TESSEL CH formulation and the six VG soil texture classes in HTESSSEL. In TESSEL those were not allowed to fall below their wilting point values. At saturation, TESSEL has the highest diffusivity and conductivity. The reduced values for fine soils in HTESSSEL reduces the infiltration of water and consequently the baseflow.

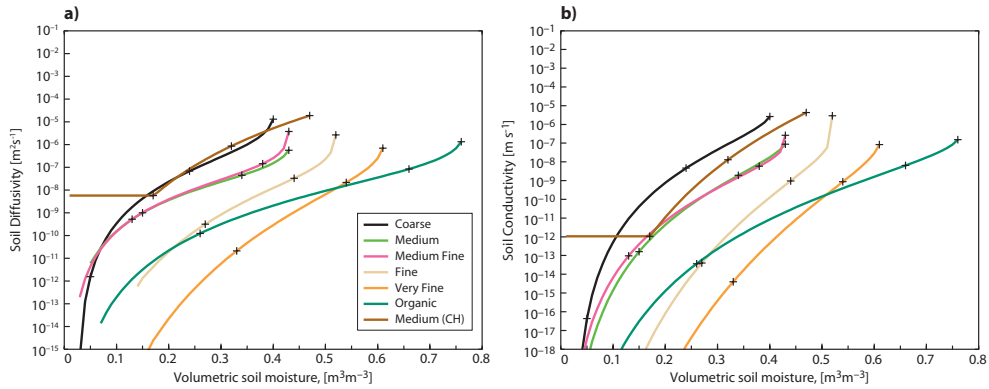


Figure 2: Hydraulic properties of TESSEL and HTESSEL: (a) Diffusivity and (b) conductivity. The (+) symbols on the curves highlight (from high to low values) saturation, field capacity permanent wilting point.

A variable infiltration rate, first introduced in the so-called Arno scheme by Dümenil and Todini (1992), accounts for the sub-grid variability related to orography and considers that the runoff can (for any precipitation amount and soil condition) occur on a fraction  $s$  of the grid-point area  $S$ .

$$\frac{s}{S} = 1 - \left(1 - \frac{W}{W_{sat}}\right)^b \quad b = \frac{\sigma_{or} - \sigma_{min}}{\sigma_{or} + \sigma_{max}} \quad (10)$$

where  $W$  and  $W_{sat}$  are vertically integrated soil water contents ( $\theta$  and  $\theta_{sat}$ ) over the first 50cm of soil defined as an effective depth for surface runoff. Parameter  $b$  is spacially variable, depends on standard deviation of orography ( $\sigma_{or}$ ), and is allowed to vary between 0.01 and 0.5. The parameters  $\sigma_{min}$  and  $\sigma_{max}$  are set to 100m and 1000m respectively as in van den Hurk and Viterbo (2003).

The surface runoff is obtained by the Hortonian runoff formulation by integrating Eq. 10 over the gridbox.

$$I_{max} = (W_{sat} - W) + \max \left[ 0, W_{sat} \left[ \left(1 - \frac{W}{W_{sat}}\right)^{\frac{1}{b+1}} - \left(\frac{T + M}{(b + 1)W_{sat}}\right) \right]^{b+1} \right] \quad (11)$$

Whenever rain or snow melt occurs, a fraction of the water is removed as surface runoff. The ratio runoff/precipitation scales with the standard deviation of orography, and therefore depends on the complexity represented in the gridbox, as well as on soil texture and soil water content via  $W$  and  $W_{sat}$ . In Figure 3 the response to a 10mm/h

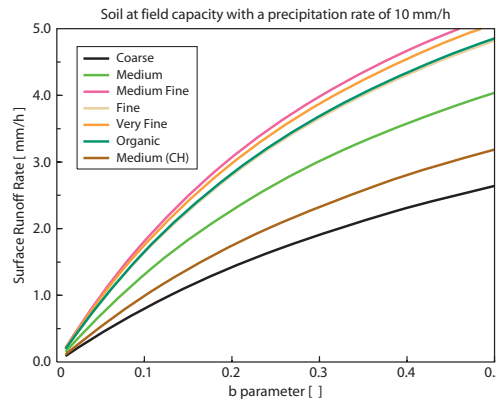


Figure 3: Surface runoff generation (rate mm/h) as a function of the  $b$  parameter (accounting for sub-grid effects of orography), when exposed to a precipitation rate of 10mm/h.

rain rate for the six VG soil types and for the CH case in TESSEL is shown as a function of the  $b$  parameter. At field capacity, the surface runoff may vary from roughly 1% to 50% of the rainfall (snow melting) rate, generally increasing with finer textures and orographic complexity.

### 3. Field site experiments

#### a. Soil properties

In order to evaluate the specified values for the permanent wilting point and field capacity used in HTESSSEL, we considered field observations of an agrometeorological network (Robock et al., 2000). These thresholds are in fact crucial to capture the seasonal and synoptic variability of soil moisture. The agrometeorologic networks operated by Russia (63 stations) and Ukraine (96 stations), as plotted in Figure 4, are used for a field-site based verification of the physiographic properties. Measurements of physical soil properties are made at a depth of



Figure 4: Geographic location of agrometeorologic stations used to evaluate soil properties.

20 cm and 100 cm and comprise the volumetric density, total water holding capacity, field capacity and level of wilting. Vegetation cover includes maize, winter wheat and spring wheat fields. Measurements are taken periodically during the agricultural season which starts at the beginning of the field work (April) and lasts until harvest time. In fields with a spatially inhomogeneous soil structure, several cross-sections are made to get a reliable estimate of these quantities.

Figures 5 and 6 show the histogram of differences between the wilting level, the field capacity and the water holding capacity (i.e. the difference between field capacity and wilting level) based on the field observations at 20cm depth. The first panel (top) shows the histograms for the FAO soil texture derived values for the field capacity calculated by setting  $\psi(\theta_{\text{cap}}) = -0.10$  bar (top panel). The second panel (middle) shows the same data, but the field capacity was set to  $\psi(\theta_{\text{cap}}) = -0.33$  bar. The bottom panel shows the histograms for the uniform soil parameters used in the TESSEL scheme. The bias observed in the wilting point of the FAO soil map is clearly substantially smaller than the bias of the uniform value used for the wilting point in TESSEL. For both networks the bias decreases by 50% or more when considering HTESSSEL, with values 3.0 vol% and 1.1 vol% for Ukraine and Russia respectively (for TESSEL the bias is 6.2 vol% and 3.4 vol%). For the field capacity the results depend largely on the setting of  $\psi(\theta_{\text{cap}})$ . Setting the value to  $-0.10$  bar leads to differences similar to those observed for TESSEL. For the Ukrainian data the absolute bias slightly increases by 1.3 vol%; for Russia the absolute bias decreases by 1.2 vol%. Although Hillel (1982) indicate a matric potential  $\psi(\theta_{\text{cap}})$  of  $-0.33$  bar as a common value for medium-textured soil field capacity, this leads in HTESSSEL to a substantial degradation when compared to the field capacity estimates. The bias increases to a high value of  $-4.7$  vol% and  $-5.4$  vol% for Ukraine and Russia respectively. These biases are significantly larger than those observed for the

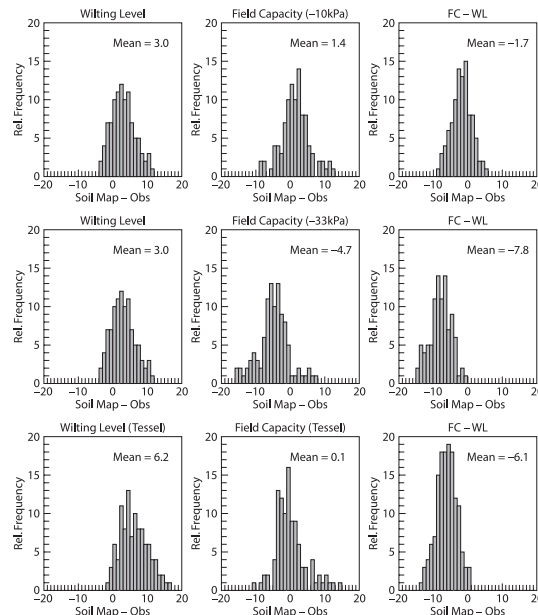


Figure 5: Histograms of differences between soil properties observed at stations of the Ukrainian agrometeorologic network. Differences are calculated for the wilting level, the field capacity and the water holding capacity. The top panel compares HTESSEL to field observations with  $\psi(\theta_{cap}) = -0.10$  bar; the middle panel compares HTESSEL to field observations with  $\psi(\theta_{cap}) = -0.33$  bar; and the bottom panel compares the TESSEL data (with a uniform soil type) to field observations.

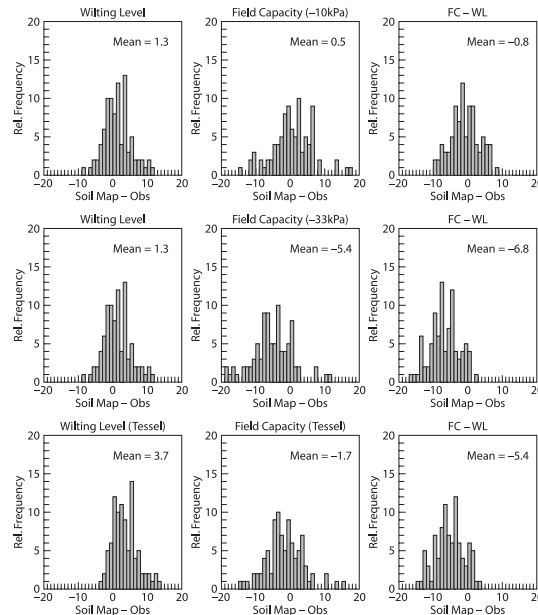


Figure 6: As Fig. 5 but for stations of the Russian agrometeorologic network.

uniform TESSEL value. Therefore the value of  $-0.10$  bar used for coarse textured soil is adopted for all the soil texture classes. The water holding capacity reflects the positive impact of this choice and of the new soil scheme. For both networks the bias decreases significantly for the HTESSEL scheme.

*b. Soil moisture and fluxes*

The validation focuses on well instrumented sites where various types of observations are available and where the soil type was likely to play a significant role in the surface model behaviour. Long time series (one year or more) of hourly observations of low level wind, temperature and moisture, together with precipitation and downward radiation are used as input to the land surface. Two different sites are considered for offline simulations using both TESSEL and HTESSEL. Table 3 reports the location and the physiography (soil and vegetation) for each site. These quantities were assigned by the operational high resolution forecast model (at about 25km globally) adopting the nearest gridbox. The sites correspond to different soil textures and to extremely

Table 3: Field site experiments considered for offline validation and their physiographic properties: vegetation classes for high (TVH, 19=Interrupted forest, 5=Deciduous broadleaf) and low vegetation (TVL, 1=Crops and mixed farming, 7=Tall grass) with respective coverage (CVH and CVL). Soil texture class is according to Table 1.

Site	Lat	Lon	slt	TVH	CVH	TVL	CVL
Units	°	°	-	-	-	-	-
SEBEX	13.500	1.500	1	19	0.45	7	0.55
BERMS-OA	53.629	-106.198	3	5	0.79	1	0.21

constrasting climatic conditions. The initial conditions for the land surface state including soil moisture have been obtained via perpetual-year integrations until the schemes reach equilibrium.

*i. SEBEX Sahel* The Sahelian Energy Balance EXperiment (Wallace et al., 1991) is characterized by a desert climate with fallow savannah vegetation and sandy soil. Volumetric soil moisture reaches extremely low values in the dry season. This dynamical range is typical for sandy soil and can not be represented by the medium texture used in TESSEL, resulting in a much wetter range. Observations of both soil moisture and evaporation are available for verification, as previously considered in van den Hurk et al. (2000). Figure 7 shows the time

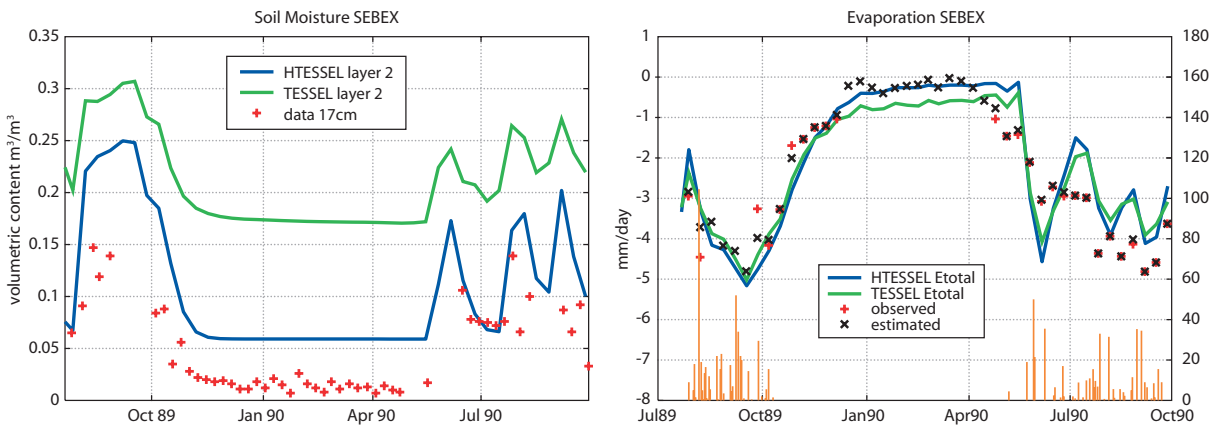


Figure 7: TESSEL (green line) and HTESSEL (blue line) compared to observations (red +) and local estimates (black x): (Left:) Volumetric soil moisture; and (Right:) Evaporation (negative for upward fluxes). The bars indicate daily precipitation in mm (right hand scale).

series of soil moisture. It is clear that the soil moisture range is much better represented by the HTESSEL scheme. This results also in a slightly better match for evaporation during the dry season. TESSEL retains too much water for this desert savannah site.

ii. *BERMS Boreal Forest* The BERMS Old Aspen site located in Canadian Boreal forest (central Saskatchewan) has a high soil water retention. The data have been used for the validation of fluxes from ERA-40 in [Betts et al. \(2006\)](#). BERMS data represents one of the longest comprehensive time-series available for land surface model verification. It has a marked interannual variability, allowing the evaluation of multiple time scales. Compared to the SEBEX site, TESSEL soil texture (medium) properties are closer to HTESSEL (medium-fine, according to FAO). Still, both the absolute values and the interannual variability of soil moisture are better captured by the HTESSEL as shown in Figure 8. This is explained by a more appropriate soil texture and by the increased

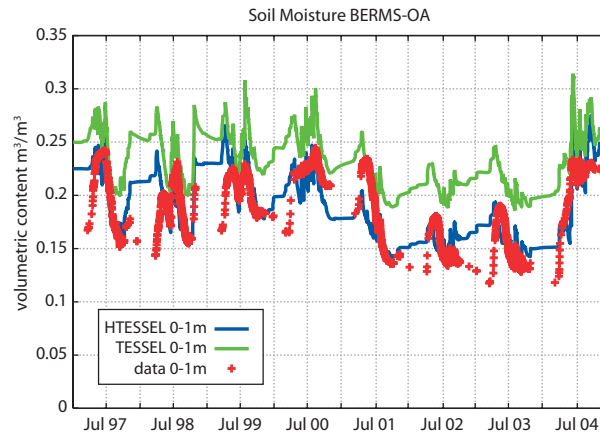


Figure 8: Volumetric soil moisture in TESSEL (green line) and HTESSEL (blue line) compared to observations (red +) for BERMS Old Aspen Boreal forest Canada.

memory in the Van Genuchten hydrology scheme. In fact according to Figure 2, the conductivity is greatly reduced for all the soil texture classes except coarse textured soils, leading to a much longer recharge/discharge period.

#### 4. Offline regional and global simulations

The verification of the models' hydrology for large domains is a complex task. This is due both to the lack of direct observations and to a composite effect of shortcomings in land surface parametrizations, which produce errors not easily traced to a single process. Global atmospheric re-analyses (ECMWF Re-Analysis series, ERA15, ERA-40, ERA-Interim, National Centers for Environmental Predictions-Department of Energy, NCEP-DOE Reanalysis, Japanese Re-Analysis, JRA25) offer an estimate of water budgets on the global domain. However, those estimates are heavily model-dependent and known to have deficiencies either in the land surface scheme or in the surface fluxes. This limits the validity for quantitative estimates. [Seneviratne et al. \(2004\)](#) and [Hirschi et al. \(2006a\)](#) bypassed the strong dependence on the land surface model formulation used in the reanalysis system by considering the water budget of large basins using both atmospheric moisture convergence fields derived from reanalysis and observed river-discharge. Water balance closure can be thus calculated without the use of atmospheric model precipitation and evaporation from the land surface model. A Basin Scale Water Budget (BSWB) dataset has been gathered for major World river catchments. Considering hydrology over large domains allows the verification of subgrid-scale parameterizations (e.g. runoff) that can not be evaluated at single instrumented sites, and the assessment of the overall behaviour of the scheme, which may be hidden in field site experiments (lack of representativity). We focus essentially on runoff and terrestrial water storage changes to validate the performance of HTESSEL and TESSEL. Monthly time-scales are considered for the largest catchments (mainly in the Northern hemisphere). Runoff at daily time-scales is evaluated on a well-known catchment experiment, RhôneAgg ([Boone et al., 2004](#)).

a. *The GSWP-2 experiment*

The Global Soil Wetness Project, Second initiative, GSWP-2 (Dirmeyer et al., 1999, 2002; Gao et al., 2004) provides a set of near-surface forcing to drive land surface schemes offline. GSWP-2 covers the period July 1982 to December 1995. The atmospheric forcing data are provided at a resolution of  $1^\circ$  globally on a domain of  $360 \times 150$  grid-points and does not consider latitudes south of  $60^\circ\text{S}$ . The GSWP-2 data were originally based on atmospheric reanalyses (NCEP-DOE Reanalysis) at 3-hour intervals, corrected using observational data as detailed in (Dirmeyer et al., 2002). For the current experiments we have used the latest release of GSWP-2 atmospheric forcing based on ERA-40 where only precipitation is corrected using the Global Precipitation Climatology Project (GPCP) dataset. These fields are labelled ERAGSWP. Temperature and pressure fields are rescaled according to elevation differences between the reanalysis model topography and that used in GSWP-2, while surface radiation and wind fields are unchanged. The state variables of surface pressure, air temperature and specific humidity at  $2m$ , as well as wind at  $10m$  are provided as instantaneous values. The surface radiation and precipitation flux represent 3-hour averages. The GSWP-2 forcings are linearly interpolated in time to the integration timestep of 30 minutes. The 10-year runs are aggregated into monthly climatologies and considered over large catchments.

i. *Terrestrial water storage* The variation of the terrestrial water storage ( $TWS$ ) can be expressed as:

$$\frac{dTWS}{dt} = P + E + R \quad (12)$$

where  $P$ ,  $E$ ,  $R$  are the precipitation, evapotranspiration and runoff respectively.  $TWS$  accounts from both snow-pack and soil moisture variations. As previously mentioned, Eq. 12 can be combined with the atmospheric water balance to eliminate the  $P$  and  $E$  terms which in atmospheric reanalysis are only indirectly constrained by observations and strongly rely on model estimates. The expression obtained is

$$\frac{dTWS}{dt} = -\frac{dW}{dt} - \nabla Q + R \quad (13)$$

where the terms  $\frac{dW}{dt}$  (atmospheric total column water variations), and  $-\nabla Q$  (atmospheric moisture convergence), are taken from ERA-40 reanalysis and are thus directly constrained by assimilated observations (e.g. radiosondes). The runoff  $R$  is obtained by the observed river discharge from the Global Runoff Data Centre (GRDC) divided by the basin area.

The  $TWS$  estimates in the BSWB dataset, obtained from Eq. 13, are shown to correlate well with land surface soil moisture observations averaged on large domains. Moreover, mass variations detected from the GRACE satellite mission correlate reasonably well with  $TWS$  (Hirschi et al., 2006b). In the GSWP-2 simulations, the  $TWS$  variations are computed directly from the monthly means of total column soil moisture variations and the snow water equivalent variations. A number of Central European catchments are selected to show the effect of the revised hydrology. An improved description of the  $TWS$  change in HTESSSEL-offline can be seen in Figure 9, both when compared to ERA-40 (in which TESSEL is used in a coupled mode) and TESSEL-offline (driven by ERAGSWP forcing). The reason for this improvement with respect to ERA-40  $TWS$  is discussed in Section 5.3. The slightly larger amplitude of  $TWS$  annual cycle in HTESSSEL is mostly associated to the increased water holding capacity, as reported in Table 2.

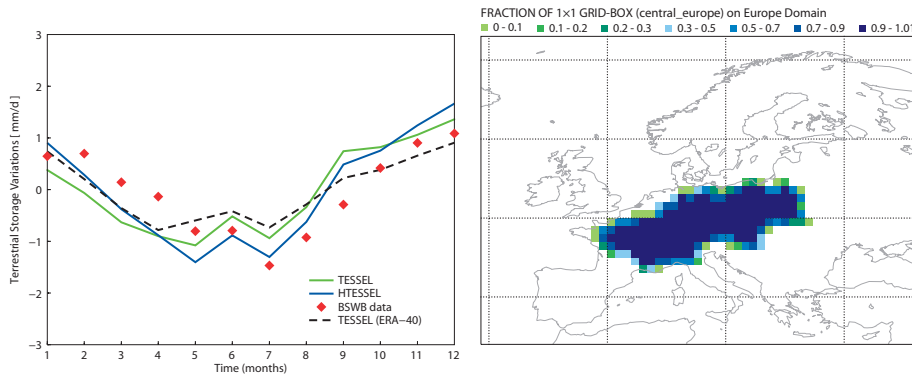


Figure 9: Monthly Terrestrial Water Storage (TWS) changes (a) on Central European catchments (b): Wisla, Odra, Elbe, Weser, Rhine, Seine, Rhône, Po, North-Danube) for TESEL (GSWP-2-driven, green line), HTESEL (GSWP-2-driven, blue line), TESEL in ERA-40 (black dashed line) and BSWB data (red diamonds) for 1986-1995.

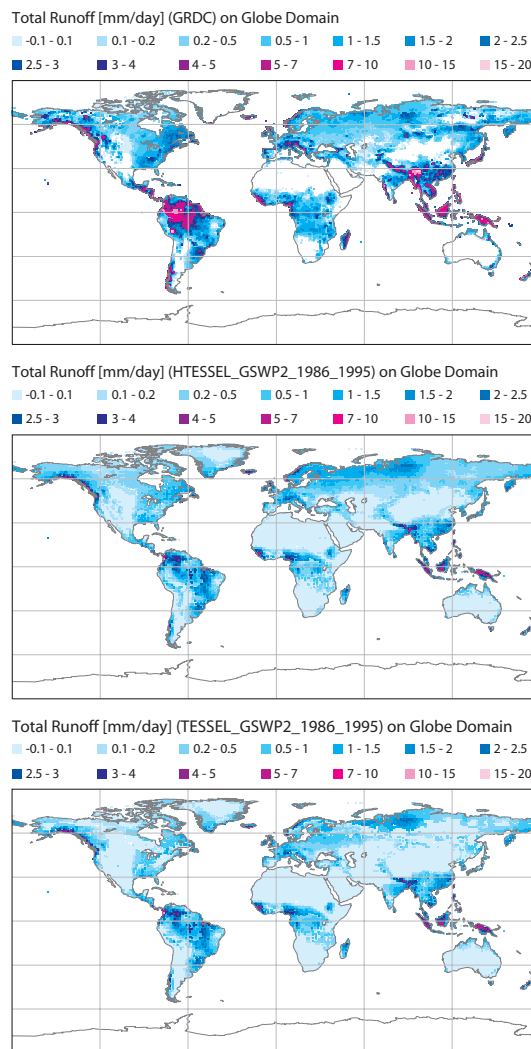


Figure 10: Total runoff from GRDC composite (top panel) HTESEL (middle) and TESEL (bottom) for the decade 1986-1995

ii. *Monthly runoff* The Global Runoff Data Centre operates under the auspice of the World Meteorological Organization and provides data for verification of atmospheric and hydrologic models. The GRDC database is updated continuously, and contains daily and monthly discharge data information for over 3000 hydrologic stations in river basins located in 143 countries. Over the GSWP-2 period the runoff data for 1352 discharge gauging stations were available. A  $0.5^\circ$  regular-grid mean annual runoff product is provided by the GRDC (<http://www.grdc.sr.unh.edu/>). This product is produced with an underlying precipitation climatology (Fekete et al., 2000), which is readjusted whenever the observed runoff exceeds the input precipitation. Given the large number of assumptions involved in the production of a global runoff climatology and particularly for precipitation in ungauged basins, only a qualitative comparison is appropriate. Figure 10 shows the comparison of HTESSEL and TESSEL with the GRDC product. Improvements are mainly visible in the Northern Hemisphere, where the non-zero runoff area is significantly increased in HTESSEL, consistent with GRDC. The limitations of ERA-GPCP precipitation dataset (used to force the stand-alone simulations) are clearly visible in the tropical belt. In fact, a strong underestimation of rainfall (as reported in Betts et al. 2005 for Amazon basin) produces noticeable effects on the simulated annual runoff: both HTESSEL and TESSEL greatly underestimate the GRDC runoff rates in this areas.

A basin-scale evaluation is considered as well. It is appropriate for large basins which are reasonably well gauged and where the time-delay of the water path (routing) does not limit the validity of the comparison (e.g. excluding therefore the Amazon where the routing plays a major role in timing the runoff). Figure 11 shows the errors of the monthly runoff evaluated on 41 different basins, listed in Table 4. RMSE and BIAS are calculated on the (TESSEL and HTESSEL) monthly runoff against the GRDC monthly runoff estimates. The

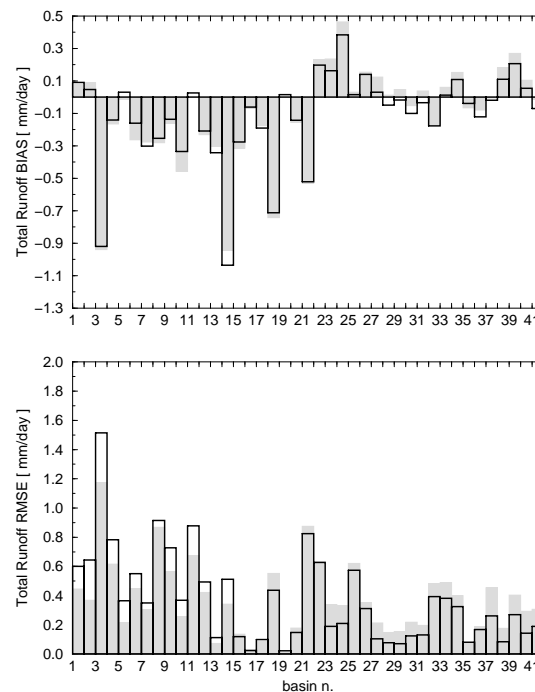


Figure 11: Total runoff verification on basins against GRDC river discharge: BIAS (top) and RMSE (bottom). Shown are HTESSEL (black line) and TESSEL (grey shading).

Table 4: List of basins considered for the runoff verification

N.	Basin	N.	Basin
1	Ob	22	Volga
2	Tura	23	Don
3	Tom	24	Dnepr
4	Podkamennaya-Tunguska	25	Neva
5	Irtish	26	Baltic
6	Amudarya	27	Elbe
7	Amur	28	Odra
8	Lena	29	Wisla
9	Yenisei	30	Danube
10	Syrdarya	31	Northeast-Europe
11	Yukon	32	Po
12	Mackenzie	33	Rhine
13	Mississippi	34	Weser
14	Ohio	35	Ebro
15	Columbia	36	Garonne
16	Missouri	37	Rhône
17	Arkansas	38	Loire
18	Xhangjiang	39	Seine
19	Murray-darling	40	France
20	Selenga	41	Central-Europe
21	Vitim		

HTESSEL simulation shows an overall reduction of the mean BIAS for most basins (with the Ohio river basin, n. 14 in Figure 11, being a noticeable exception). For RMSE, roughly a third of the basins (N. 1-14) register a net deterioration, while the majority shows a marked improvement. This behaviour can be explained from the effect of snow ablation. The TESSEL snow treatment (not modified in HTESSEL scheme) suffers from the lack of a refreezing mechanism for water in the snow-pack, which activates the runoff too quickly and produces a pronounced peak.

Although the RMSE of the monthly runoff has deteriorated for snow-dominated basins, the BIAS is generally reduced. The magnitude of the spring runoff peak is also in a better agreement with observations for HTESSEL as shown in Figure 12 for the Yenisei Siberian basin (n. 9 in Figure 11). The correct timing will only be achieved by a revision of the snow scheme. The link between snow and soil moisture errors is discussed further in Section 5.3.

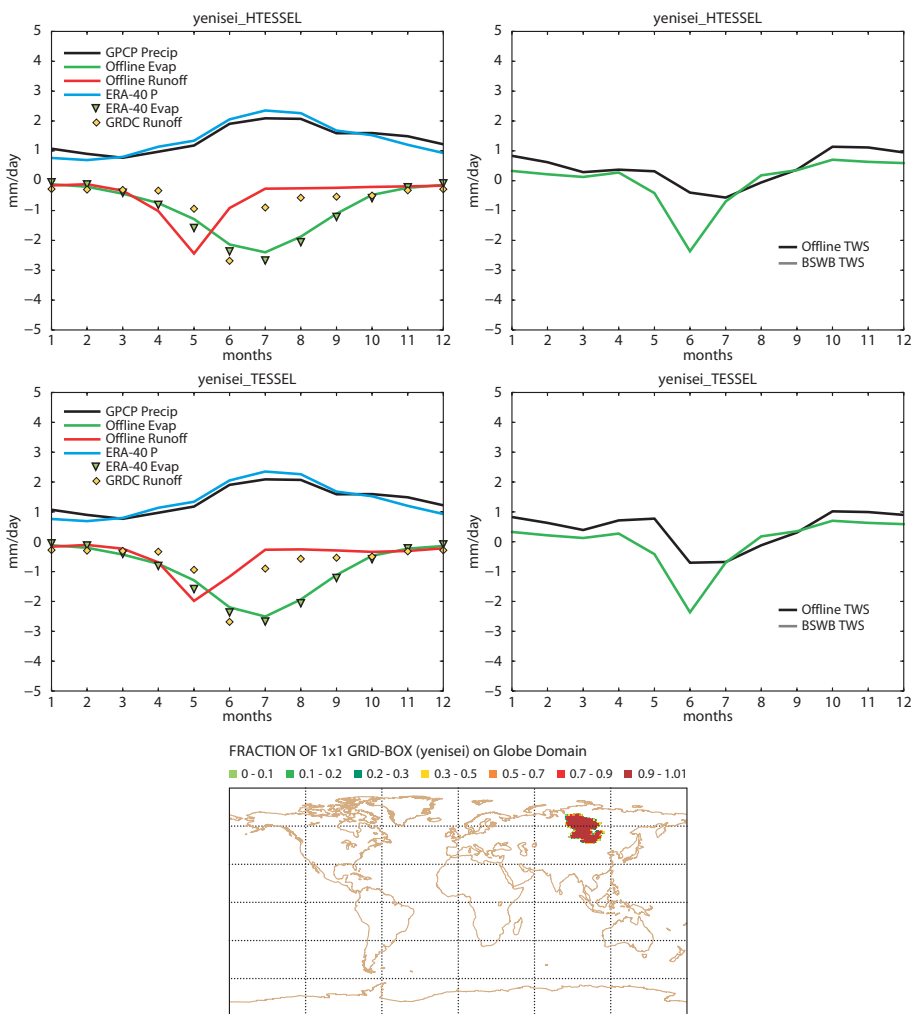


Figure 12: Yenisei water budget for HTESSEL and TESSEL during the GSWP-2 period (1986-1995) compared with BSWB, GRDC and ERA-40 estimates.

### b. The RhôneAgg experiment

Earlier evaluations of predecessors of HTESSEL were carried out in the context of the so-called RhôneAgg experiment (Boone et al., 2004). This experiment was designed to test the effects of spatial aggregation between fine scale and coarse scale grids for hydrological simulations of a complex terrain like the Rhône catchment valley ( $95000\text{km}^2$ ). Similar to the GSWP-2 set-up, a 3-hourly forcing was provided for the domain at different resolutions ( $8\text{km}$  and  $1^\circ$ ) for a 4-year period (1 August 1985 to 1 August 1989). The first year was considered to be a spin-up year. Verifying daily discharge data were also made available for a number of sub-catchments and the major Rhône branch at Viviers. At daily time scales, river routing of the modelled runoff generation greatly

Table 5: RMSE and Nash-Sutcliffe scores for the Rhône basin for TESSEL and HTESSEL and their delayed output versions

Version	RMSE ( $\text{m}^3\text{s}^{-1}$ )	Nash-Sutcliffe
TESSEL	692	0.32
TESSEL delayed output	768	0.12
HTESSEL	825	0.02
HTESSEL delayed output	720	0.21

affects the results for catchments of the size of the Rhône basin. The RMSE and Nash-Sutcliffe scores of daily discharge data for this limited time period are worse for HTESSEL than for TESSEL (Table 5). Scores are calculated by direct comparison of modelled surface runoff generation to daily discharge measured at Viviers, and therefore are clearly penalizing the scheme with greater variability but still lacking a routing scheme. A detailed routing scheme was not available, but a crude estimate of the grid point dependent delay between the modelled runoff generation and the outlet in Viviers was made by assuming a fixed channel propagation speed ( $100\text{ km/day}$ ) over the (shortest) distance between the grid point and the outlet position. Delay times were rounded to whole days (up to 6 days for the upper north part of the basin). This procedure (denoted by delayed output in Table 5) clearly improves the RMSE and Nash-Sutcliffe scores for HTESSEL, and deteriorates the TESSEL output.

Apart from the objective statistical scores, a clear effect of the subgrid runoff scheme on the time series of the simulated discharge is visible in Figure 13. The high frequency variability in TESSEL is significantly lower than in HTESSEL (see also the spectrum shown in Figure 14). The runoff delay from the grid points far from the outlet has a strong impact on the time series at the outlet both for TESSEL (Figure 13) and HTESSEL (Figure 14). A strong smoothing is caused by the delayed output produced by TESSEL. Apparently, peaks generated by saturated grid boxes receiving additional precipitation or melt events are compensated by grid boxes with low runoff generation, and virtually all major peaks are removed. In HTESSEL the delayed output causes a much better resemblance of the modelled power spectrum to the observations (Figure 14). Without the output delay, the power at high frequencies is too high in HTESSEL, and this overestimation is effectively removed. The contribution of high frequencies to the overall signal variance in TESSEL is clearly underestimated. Monthly discharge for the Rhône basin simulated in the GSWP-2 context resulted in a clear improvement of the RMSE score (from  $0.45\text{mm/day}$  for TESSEL to  $0.26\text{mm/day}$  for HTESSEL) and had virtually no impact on the bias.

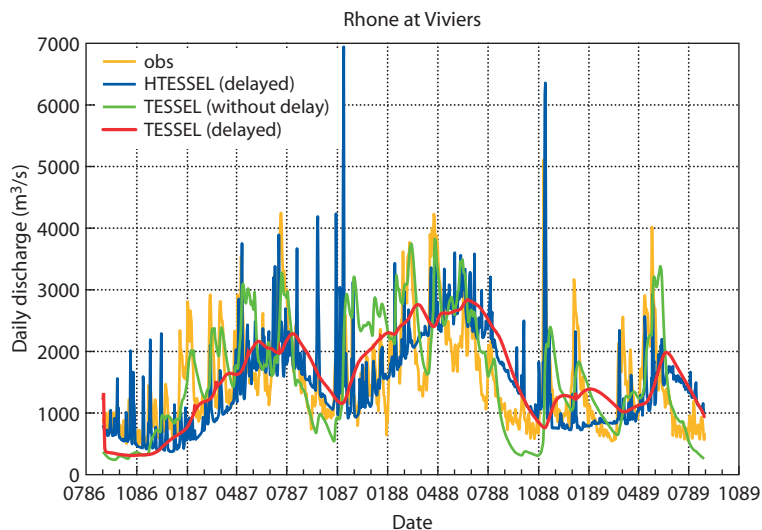


Figure 13: Simulated and observed daily discharge at Viviers. Shown are model results for HTESSEL (with the delayed output being effective) and TESSEL both with and without the delayed output.

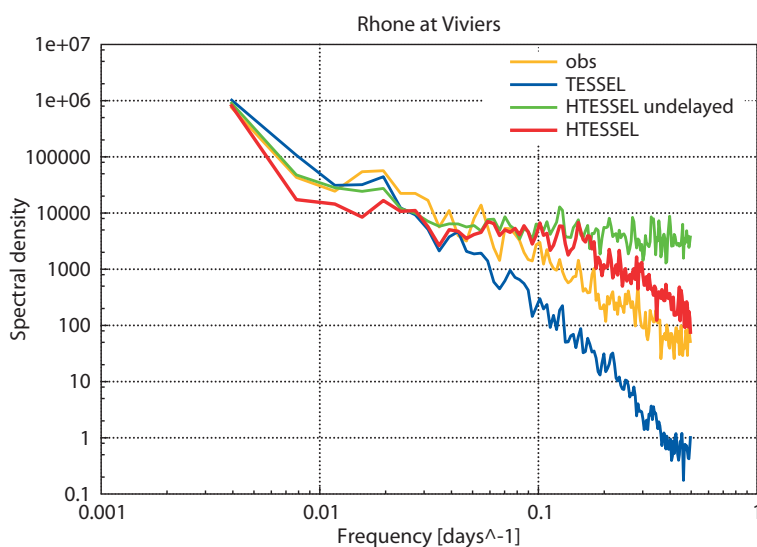


Figure 14: Power spectrum of the observed and modelled daily discharge of the Rhône basin for the entire simulation period.

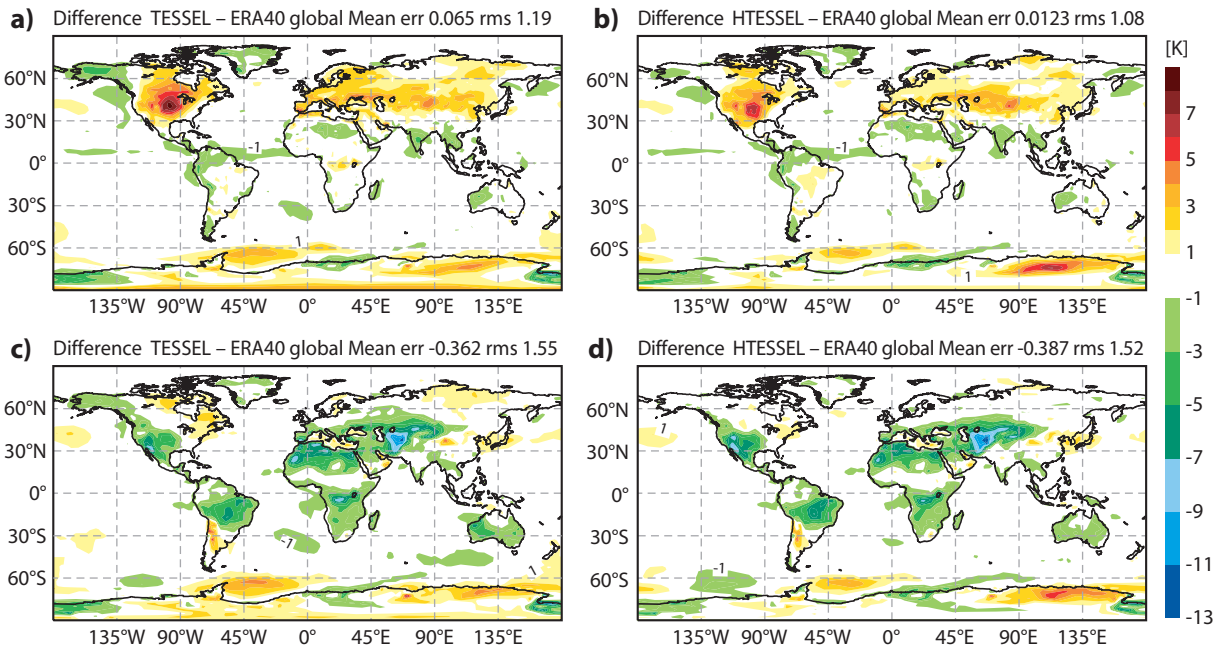


Figure 15: Climate experiments, impact on 2m temperature (upper panels) and 2m dew point temperature (lower panels): (a, c) TESSEL, (b, d) HTESSEL. Shown are the mean 2m errors for JJA model climate evaluated against ERA-40.

## 5. Atmospheric-coupled simulations

Global atmospheric coupled experiments are used to evaluate the land-atmosphere feedback especially on near-surface atmospheric quantities. Various ensemble sets of multi-month integrations are performed. We refer to these integrations as *climate simulations*. Short term predictions (12-hour) embedded in long data assimilation cycles (several months) are also used to evaluate the analysis increments, as a measure of model improvements.

### a. Climate simulations

Two sets of climate simulations have been performed, using an atmospheric model configuration with 91 vertical layers and a grid-point resolution of about 120km (truncation T159 of a gaussian reduced grid). A 13-month 4-member ensemble for the period 01/08/2000 to 31/08/2001, and a multi-year 10-member ensemble of 7-month runs (starting April 1 each year from 1991 to 1999) were executed. The experiments showed a very small atmospheric response to the land surface scheme modifications. A slightly positive impact is seen in temperature at 2m compared with ERA-40 climatology as shown in Figure 15. The 2m temperature RMSE error is reduced from 1.19K to 1.08K, while the 2m dew-point temperature error is unchanged. The error patterns are similar for both 2m temperatures, and the error reduction in the HTESSEL simulation (Figure 15b and d) is mostly concentrated in Northern Hemisphere continental areas.

### b. Extended Data Assimilation experiments

Considering the land surface water budget during a data assimilation cycle, Eq. 12 becomes

$$\frac{dTWS}{dt} = P + E + R + \delta A \quad (14)$$

where  $\delta A$  represents the analysis increments (in snow  $\delta S_n$  and soil moisture  $\delta \theta$ ) added for each cycle of the data assimilation system. It is assumed that a better land surface hydrology will lead to smaller systematic increments  $\delta A$ . We compared the increments for two data assimilation cycles with TESSEL and HTESSSEL as land surface schemes. For HTESSSEL, the Optimum Interpolation (OI) soil moisture analysis (Mahfouf, 1991; Douville et al., 2000; Mahfouf et al., 2000) has also been revised for consistency. The OI coefficients have been rescaled according to the ratio of water holding capacity in HTESSSEL, a function of local soil texture, to the constant value in TESSEL (see Table 2).

In order to focus on timescales relevant for the land-surface processes, we considered a 7-month period covering the boreal summer (01/04/2006 to 31/10/2006). The analysis makes use of short-term forecast errors in 2m temperature and relative humidity to correct soil moisture errors via a set of (OI) coefficients (see Douville et al. 2000 for the detailed formulation). The absolute difference (HTESSSEL - TESSEL) of the soil moisture analysis increments over summer (JJA) is shown in Figure 16. Generally, a reduction of the mean daily soil moisture increments is observed at mid-latitudes, particularly over Europe and the central U.S. where the SYNOP network is dense and the OI analysis most effective. This signal confirms the positive impact of HTESSSEL over these areas, certainly when we recall that the dynamical range of soil moisture is greatly increased. Northern regions, show larger SM analysis increments in HTESSSEL for the month of June, associated with land surface spin-up from previous snow-cover, frozen soil conditions. Increments are mostly reduced in August (Figure 16c).

### c. ERA-40 analysis increments and lesson learnt

The long ERA-40 dataset with a frozen configuration of the data assimilation and modelling systems, provides the opportunity to produce valuable diagnostics on data assimilation increments. It turns out that the soil moisture and snow mass errors are tightly coupled at high latitudes. In ERA-40, the snow mass is analysed from SYNOP snow depth observations, with relaxation to climatology (12-day time scale) as a constraint in data-sparse areas. Systematic soil moisture/snow mass analysis increments indicate deficiencies in the system, which can be due to data or model errors, or due to a suboptimal data assimilation. Figure 17 shows the monthly mean data assimilation increments (expressed in mm/day) for snow and soil moisture, calculated from ERA-40 and evaluated for the decade 1986-1995 (consistent with the GSWP-2 period). Results are presented in the form of a Hovmöller diagram (land-only zonal means as a function of latitude and month of the year). Focusing on northern latitudes, the snow analysis increments moving from  $40^\circ N$  in winter to  $70 - 80^\circ N$  in June indicate a persistent positive correction which is attributed to the early melting of snow. This pattern is mirrored in the soil moisture analysis which removes the water supply. The snow depth increments and the associated soil moisture increments clearly suggest that the model is melting the snow too early, which is consistent with the offline simulations as shown in Figure 12. In the latter case, the snow melt results in a runoff peak which is one month too early compared to the observations.

At mid-latitudes during the boreal summer months, positive soil moisture analysis increments are systematic (Figure 17), which suggests that the land surface model has a tendency of running dry in summer. From budget diagnostic on the European basins we know that the amplitude of the seasonal cycle of TWS-change in ERA-40 is much smaller than observed (Figure 9). This is also concluded by Drusch and Viterbo (2007) by comparing analysed soil moisture with in situ observations. More insight can be gained by considering, for the same basin, the water budget terms of Eq. 14 in stand-alone simulations with GSWP2 forcing and in ERA-40 (Figure 18). It is shown that much of the summer increments (up to 1 mm/day) in ERA-40 are a response to the precipitation deficit in the short range forecasts of ERA-40 (also confirmed by van den Hurk et al., 2008). It is interesting that both systems, i.e. ERA-40 affected by biased precipitation and with large data assimilation increments, and the stand-alone simulation with more realistic precipitation and no data assimilation, simulate very similar evaporation. Still the amplitude of the seasonal cycle of TWS is smaller in the ERA-40 system than in the

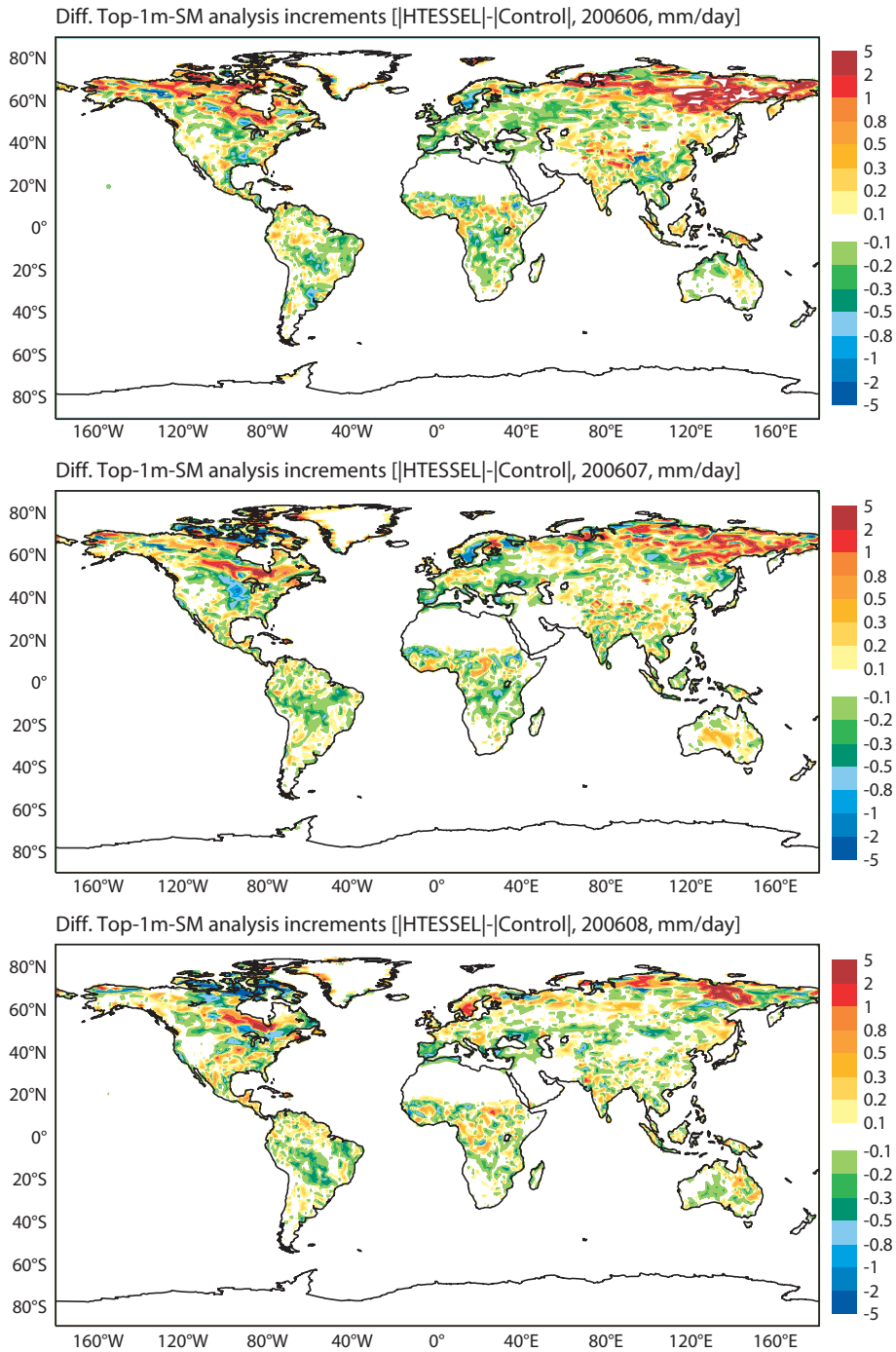


Figure 16: Absolute difference in the daily soil moisture analysis increments between HTESSEL and TESSEL (Control) for the months of June, July, and August 2006 (top to bottom panels).

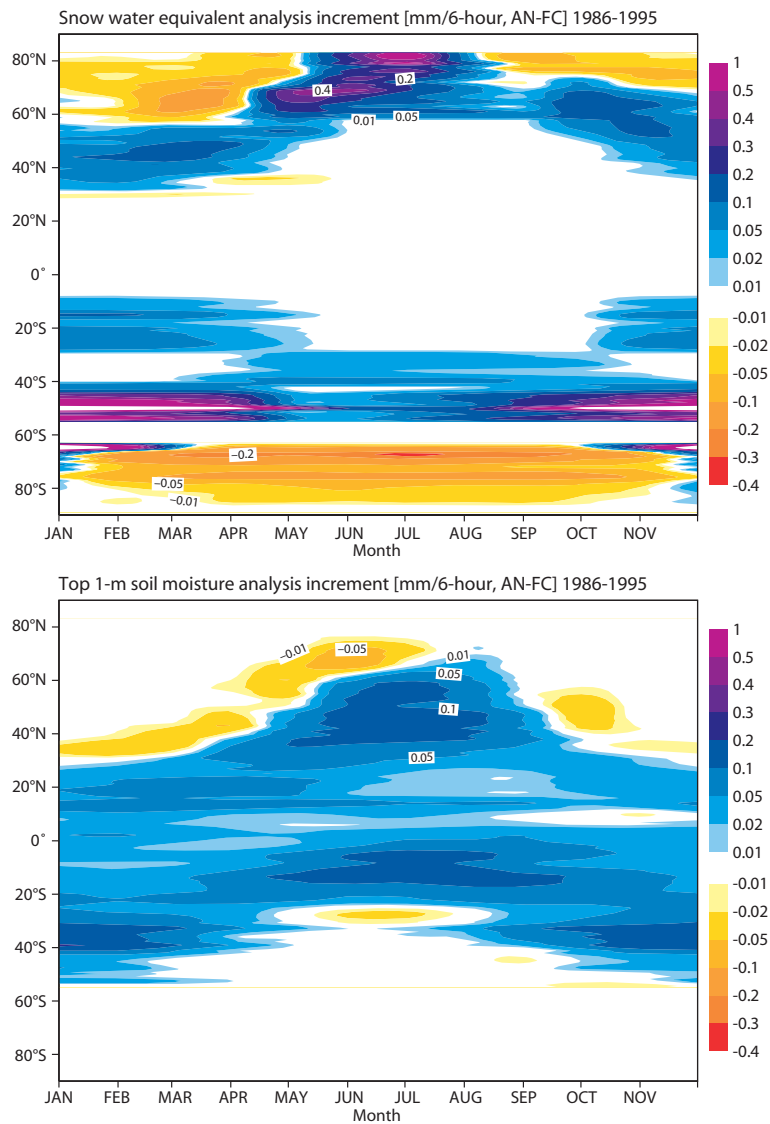


Figure 17: Monthly average soil moisture and snow analysis increments in ERA-40 calculated on the 1986-1995 decade.

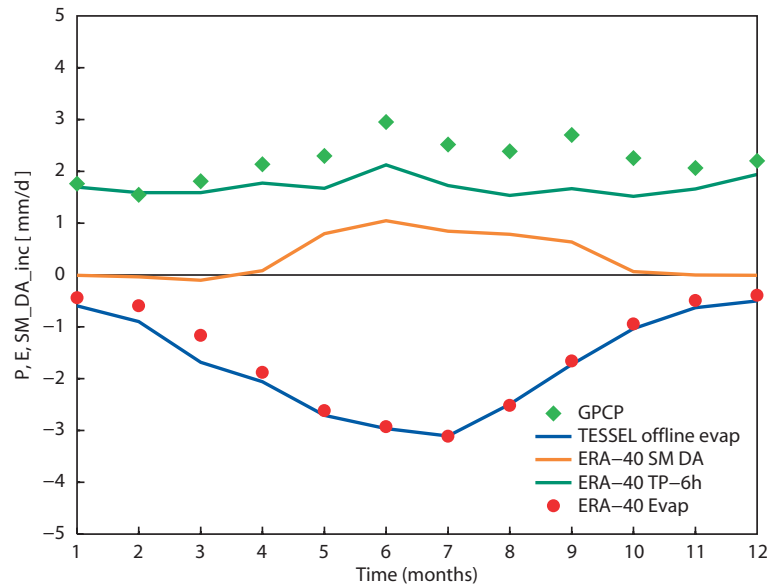


Figure 18: Surface water budget for the area in Fig. 9: ERA-40 precipitation (green line) and GPCP data (green diamonds). Soil moisture analysis increments (orange line). Offline (GSWP-2-driven) TESSEL evaporation (blue line) and ERA-40 evaporation (red circle).

stand-alone simulations (consistent with the results of Ferranti and Viterbo, 2006). Having similar evaporation with different soil moisture may sound contradictory. Apparently the lack of precipitation is over-corrected by data assimilation increments, suggesting that the data assimilation might be suboptimal.

The conclusion we draw here is that data assimilation increments are a valuable diagnostic. They obviously indicate a deficiency in the system in the sense that somehow the model is not capable of matching the observations. Particularly when the control variable (e.g. soil moisture) is rather different from the observable (e.g. 2m temperature and humidity) and the model becomes very important. However, data assimilation increments by themselves do not indicate the cause of the problems. In the case of ERA-40, it turned out particularly helpful to be able to do stand-alone simulations with observed precipitation. Both the precipitation bias and the suboptimal data assimilation contribute to the rather large soil moisture increments, which are affecting the evolution of the TWS cycle.

## 6. Summary and Conclusions

A revised hydrology for the ECMWF land surface scheme (HTESSEL) is tested and compared against observations from field site experiments. The revision is introduced to correct two main shortcomings of the land surface scheme: the absence of surface runoff and a global uniform soil texture. A new dataset for soil type is included by assigning a hydrological class (up to six) to each grid cell. A revised infiltration scheme with sub-grid surface runoff description is also introduced and evaluated. In point comparisons with field site experiments these modifications show a shift in the soil moisture range to give better agreement with observations. The soil physiographic parameters (wilting point and field capacity) associated to each soil texture produce a larger water holding capacity. In drylands the shift of the soil moisture range gives slightly better evaporation. A Boreal forest site is selected for its long time-series of soil moisture observations. The inter-annual variability of root-zone soil moisture in a boreal forest site shows improvements with a satisfactory match to the 8-year dataset. The improved match of soil moisture to observed values is a necessary step towards the improved

assimilation of satellite data such as microwave radiances. In conclusion, the proposed changes to the ECMWF scheme address known short-comings without affecting the generally good performance of the land surface model in providing the lower boundary conditions to the atmospheric model.

A set of regional stand-alone experiments (GSWP-2, 1986-1995) is used to evaluate the terrestrial water storage variations over the Central European river-basins in comparison with independent estimates based on atmospheric moisture convergence data and river discharge observations. The model global annual runoff map shows some small improvement when compared with the river discharge product. Quantitative evaluation of the runoff at monthly time-scales shows a net improvement of runoff timing in relevant catchments. In basins dominated by snow, spring snow melt is still too early, because of errors in the snow scheme. The annual BIAS in runoff is reduced for most of the basins considered. Errors in snow-melt are combined with a more active surface runoff generation in HTESSEL, and therefore lead to increased RMSE in runoff. Daily time-scale for the runoff are studied in the RhôneAgg experiment (1985-1989) where the main improvement is a spectrum of river discharge values closer to observations.

Atmospheric coupled verification is carried out using climate runs and long data assimilation experiments to evaluate the ensemble of changes in the land surface scheme and in the soil moisture analysis. At global scales, precipitation, snow and soil water errors are tightly coupled to water budget issues. Stand-alone integrations allow one to separate errors in ERA-40 terrestrial water storage largely due to precipitation deficits in the 0-6h forecast (and to a suboptimal soil moisture correction) from snow related errors which remain a feature of the new land surface scheme. The new soil hydrology appears to clearly benefit runoff and terrestrial water storage in snow-free areas. The operational implementation of a revised hydrology scheme is presented in Appendix. Future efforts to improve the annual terrestrial water balance will include adding a seasonal vegetation cycle and improving the snow scheme.

## Acknowledgements

The authors wish to thank Adrian Tompkins, Thomas Jung, Paco Doblus-Reyes, Antje Weisheimer, for the help with climate runs, Matthias Drusch and Jean-François Mahfouf for discussions on the OI data assimilation. Emanuel Dutra and Patricia de Rosnay were helpful with independent evaluation of HTESSEL and valuable discussions. Deborah Salmond, Mats Hamrud and Nils Wedi are thanked for help with IFS code, Jan Haseler and Joerg Urban for help with the scripts. Aaron Boone and Joel Noilhan are acknowledged for providing the RhôneAgg dataset and for valuable discussions. We would like to thank the UK Centre for Ecology and Hydrology, and the Fluxnet-Canada Research Network for making available the SEBEX and BERMS datasets respectively. Freddy Nachtergaele and Attila Nemes are acknowledged for help with soil texture data and valuable discussions on soil properties aggregation. Alan Betts acknowledges support from NSF through grant ATM-0529797. Rob Hine and Anabel Bowen are thanked for improving the figures appearance.

## Appendix: Global scale implementation

The Integrated Forecast System (IFS) at ECMWF include the same land surface scheme which has to operate at various spatial resolutions, conserving the main features and most importantly the same water and energy budgets. Conservation of water storage when moving across resolution is a desirable property although no scheme can easily achieve this since averaging soil (as well as vegetation) properties lead to creation/destruction of information. As illustrated, the new parameterizations proposed for the soil hydrology consider a soil type (texture) which is used to assign hydrological properties and an orographic parameter which accounts for the terrain complexity.

The FAO/UNESCO Digital Soil Map of the World, DSMW (FAO, 2003) is available at the resolution of  $5' \times 5'$  (about  $10km$ ). The FAO DSMW provides the information on two levels of soil depth  $0 - 30cm$  and  $30 - 100cm$ . The deep-soil layer ( $30 - 100cm$ ) is used to prescribe the soil texture on the soil column. when moving across resolution. The orographic runoff parameter which determines the response of surface runoff to precipitation as a function of the complexity of the terrain uses the standard deviation of orography. This quantity is already evaluated at high resolution and used in the turbulent orographic form drag (Beljaars et al., 2004). In Figure 19 the soil texture map and the standard deviation of orography are reported for the 10-day forecast operational resolution.

The soil texture and the standard deviation of orography are interpolated at various model resolutions. The standard deviation of orography can be interpolated bilinearly without special treatment. For the soil texture class interpolation, the choice of a dominant soil texture aggregation is adopted since it largely preserves the overall number of grid-points in each class. Thus water storage properties when moving across resolutions

Table 6: Percentage of soil texture class at T799 and T159 resolutions.

Texture	T799	T159
Units	%	%
Coarse	25.4	26.7
Medium	38.7	40.2
Medium-Fine	16.5	15.4
Fine	16.5	15.3
Very Fine	0.3	0.2
Organic	2.6	2.2

is also preserved without creation of information. Sand and clay percentages, often used in place of textural classes, do not conserve hydraulic properties when moving across resolutions. Table 6 shows the percentage of land points in each soil texture class at T159 (about  $100km$ ) and T799 (about  $25km$ ) resolution.

The adoption of a dominant soil texture permits an easy transition between TESSEL and HTESSSEL soil moisture, which can be obtained by a linear rescale procedure taking into account field capacity and permanent wilting point as detailed in [http://www.ecmwf.int/products/changes/soil\\_hydrology\\_cy32r3/](http://www.ecmwf.int/products/changes/soil_hydrology_cy32r3/). The soil moisture rescale between TESSEL and HTESSSEL is introduced to preserve atmospheric impact in terms of evaporation.

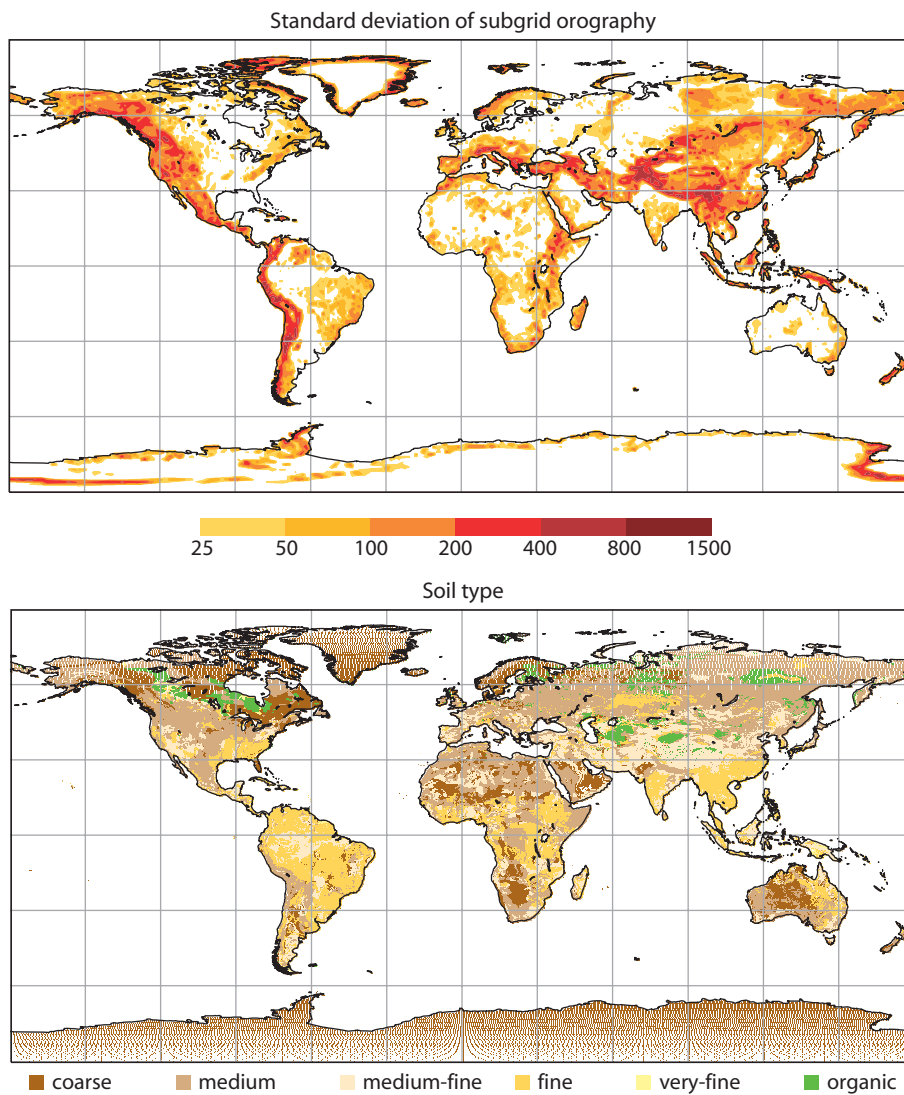


Figure 19: Standard deviation of orography (top) and soil texture (bottom) at operational resolution ( 25km).

## References

- Abramopoulos, F., C. Rosenzweig, and B. Choudury, 1988: Improved ground hydrology calculations for global climate models (GCMs): Soil water movement and evapotranspiration. *J. Climate*, **1**, 921–941.
- Beljaars, A., P. Viterbo, M. Miller, and A. Betts, 1996: The anomalous rainfall over the United States during July 1993: Sensitivity to land surface parameterization and soil moisture anomalies. *Mon. Weather Rev.*, **124**, 362–382.
- Beljaars, A. C. M., A. R. Brown, and N. Wood, 2004: A new parameterization of turbulent orographic form drag. *Q. J. R. Meteorol. Soc.*, **130**, 1327–1347.
- Betts, A. K., J. H. Ball, A. G. Barr, T. A. Black, J. H. McCaughey, and P. Viterbo, 2006: Assessing land-surface-atmosphere coupling in the ERA-40 reanalysis with boreal forest data. *Agric. For. Meteorol.*, **140**, 365–382.
- Betts, A. K., J. H. Ball, P. Viterbo, A. Dai, and J. Marengo, 2005: Hydrometeorology of the Amazon in ERA-40. *J. Hydromet.*, **6**, 764–774.
- Boone, A., et al., 2004: The Rhône-aggregation land surface scheme intercomparison project: An overview. *J. Climate*, **17**(1), 187–208.
- Clapp, R. B. and G. M. Hornberger, 1978: Empirical equations for some soil hydraulic properties. *Water Resources Res.*, **14**, 601–604.
- Cosby, B. J., G. M. Hornberger, R. B. Clapp, and T. Ginn, 1984: A statistical exploration of the relationships of soil moisture characteristics to the physical properties of soils. *Water Resources Res.*, **20**, 682–690.
- Deardorff, J. W., 1978: Efficient prediction of ground surface temperature and moisture, with inclusion of a layer of vegetation. *J. Geophys. Res.*, **83C**, 1889–1903.
- Dickinson, R., A. Henderson-Sellers, and P. Kennedy, 1993: Biosphere-atmosphere transfer scheme (BATS) version 1e as coupled to the NCAR community climate model. *Technical Report NCAR/TN-387 + STR*, NCAR Boulder, Colorado.
- Dirmeyer, P., A. Dolman, and N. Sato, 1999: The pilot phase of the global soil wetness project. *Bull. Am. Meteorol. Soc.*, **80**, 851–878.
- Dirmeyer, P., X. Gao, and T. Oki, 2002: The second global soil wetness project science and implementation plan. *IGPO Int. GEWEX Project Office Publ. Series*, **37**, 75 pp.
- Douville, H., P. Viterbo, J.-F. Mahfouf, and A. C. M. Beljaars, 2000: Evaluation of the optimum interpolation and nudging techniques for soil moisture analysis using FIFE data. *Mon. Wea. Rev.*, **128**, 1733–1756.
- Drusch, M. and P. Viterbo, 2007: Assimilation of screen-level variables in ECMWF's integrated forecast system: A study on the impact on the forecast quality and analysed soil moisture. *Mon. Weather Rev.*, **135**, 300–314.
- Dümenil, L. and E. Todini, 1992: A rainfall-runoff scheme for use in the hamburg climate model. *Advances in theoretical hydrology, A tribute to James Dooge. P. O'Kane*, European Geophysical Society Series on Hydrological Sciences 1, Elsevier, Amsterdam.
- FAO, 2003: Digital soil map of the world (DSMW). Tech. rep., Food and Agriculture Organization of the United Nations. Re-issued version.

- Fekete, B., C. Vörösmarty, and W. Grabs, 2000: Global, composite runoff fields based on observed river discharge and simulated water balance. *GRDC Report*, available at <http://www.grdc.sr.unh.edu/html/paper/ReportA4.pdf>.
- Ferranti, L. and P. Viterbo, 2006: The European summer of 2003: Sensitivity to soil water initial conditions. *J. Climate*, **19**, 3659–3680.
- Gao, X., P. Dirmeyer, and T. Oki, 2004: Update on the second global soil wetness project (GSWP-2). *GEWEX Newsletter*, **14**, 10.
- Hillel, D., 1982: *Introduction to Soil Physics*. Academic Press.
- Hirschi, M., S. Seneviratne, and C. Schär, 2006a: Seasonal variations in terrestrial water storage for major mid-latitude river basins. *J. Hydromet.*, **7**, 39–60.
- Hirschi, M., P. Viterbo, and S. Seneviratne, 2006b: Basin-scale water-balance estimates of terrestrial water storage variations from ECMWF operational forecast analysis. *Geophys. Res. Letters*, **33**, L21 401.
- Jacquemin, B. and J. Noilhan, 1990: Sensitivity study and validation of a land-surface parameterization using the HAPEX-MOBILHY data set. *Boundary-Layer Meteorol.*, **52**, 93–134.
- Koster, R. D., et al., 2004: Regions of strong coupling between soil moisture and precipitation. *Science*, **305**, 1138–1140.
- Loveland, T. R., B. C. Reed, J. F. Brown, D. O. Ohlen, Z. Zhu, L. Youing, and J. W. Merchant, 2000: Development of a global land cover characteristics database and IGBP DISCover from the 1km AVHRR data. *Int. J. Remote Sensing*, **21**, 1303–1330.
- Mahfouf, J.-F., 1991: Analysis of soil moisture from near-surface parameters: A feasibility study. *J. Appl. Meteorol.*, **30**, 1534–1547.
- Mahfouf, J.-F., P. Viterbo, H. Douville, A. Beljaars, and S. Saarinen, 2000: A revised land-surface analysis scheme in the integrated forecasting system. *ECMWF Newsletter*, **88**, 8–13.
- Mahrt, L. and H.-L. Pan, 1984: A two-layer model of soil hydrology. *Boundary-Layer Meteorol.*, **29**, 1–20.
- Milly, P. C. D., 1982: Moisture and heat transport of hysteretic, inhomogeneous porous media: A matric head-based formulation and a numerical model. *Water Resources Res.*, **18**, 489–498.
- Philip, J. R., 1957: Evaporation and moisture and heat fields in the soil. *J. Meteorol.*, **14**, 354–366.
- Richards, L. A., 1931: Capillary conduction of liquids through porous mediums. *Physics*, **1**, 318–333.
- Robock, A., K. Y. Vinnikov, G. Srinivasan, J. K. Entin, S. E. Hollinger, N. A. Speranskaya, S. Liu, and A. Namkhai, 2000: The global soil moisture data bank. *Bull. Am. Meteorol. Soc.*, **81**, 1281–1299.
- Seneviratne, S., P. Viterbo, D. Lüthi, and C. Schär, 2004: Inferring changes in terrestrial water storage using ERA-40 reanalysis data: The Mississippi river basin. *J. Climate*, **17**, 2039–2057.
- Shao, Y. and P. Irannejad, 1999: On the choice of soil hydraulic models in land-surface schemes. *Bound. Layer Meteorol.*, **90**, 83–115.
- Uppala, S., et al., 2005: The ERA-40 re-analysis. *Q. J. R. Meteorol. Soc.*, **131**, 2961–3012.

- van den Hurk, B., J. Ettema, and P. Viterbo, 2008: Analysis of soil moisture changes in Europe during a single growing season in a new ECMWF soil moisture assimilation system. *J. Hydromet.*, **9**, 116–131.
- van den Hurk, B. and P. Viterbo, 2003: The Torne-Kalix PILPS 2(e) experiment as a test bed for modifications to the ECMWF land surface scheme. *Global and Planetary Change*, **38**, 165–173.
- van den Hurk, B., et al., 2005: Soil control on runoff response to climate change in regional climate model simulations. *J. Climate*, **18**, 3536–3551.
- van den Hurk, B. J. J. M., P. Viterbo, A. C. M. Beljaars, and A. K. Betts, 2000: Offline validation of the ERA-40 surface scheme. *ECMWF Tech. Memo. No. 295*.
- van Genuchten, M., 1980: A closed form equation for predicting the hydraulic conductivity of unsaturated soils. *Soil Science Society of America Journal*, **44**, 892–898.
- Viterbo, P. and A. C. M. Beljaars, 1995: An improved land surface parametrization scheme in the ECMWF model and its validation. *J. Climate*, **8**, 2716–2748.
- Viterbo, P., A. C. M. Beljaars, J.-F. Mahfouf, and J. Teixeira, 1999: The representation of soil moisture freezing and its impact on the stable boundary layer. *Q. J. R. Meteorol. Soc.*, **125**, 2401–2426.
- Wallace, J. S., I. R. Wright, J. B. Stewart, and C. J. Holwill, 1991: The Sahelian Energy Balance EXperiment (SEBEX): ground based measurements and their potential for spatial extrapolation using satellite data. *Adv. Space Res.*, **11**, 31–41.
- Warrilow, D. L., A. B. Sangster, and A. Slingo, 1986: Modelling of land-surface processes and their influence on European climate. *UK Met Office Report, Met O 20, Tech Note 38*.